Eur. Phys. J. B **42**, 285–292 (2004)
DOI: 10.1140/epjb/e2004-00381-8

THE EUROPEAN PHYSICAL JOURNAL B

Coherent mesoscopic transport through a quantum dot-carbon nanotube system under two-photon irradiation

Li-Na Zhao[1] and Hong-Kang Zhao[1,2,a]

[1] Department of Physics, Beijing Institute of Technology, Beijing 100081, P.R. China
[2] Department of Physics, The University of Hong Kong, Pokfulam Road, Hong Kong, P.R. China

Received 17 October 2003 / Received in final form 5 July 2004
Published online 14 December 2004 –

Abstract. Mesoscopic transport through an ultrasmall quantum dot (QD) coupled to two single-wall carbon nanotube (SWCN) leads under microwave fields (MWFs) is investigated by employing the nonequilibrium Green's function (NGF) technique. The charging energy and junction capacitances influence the output characteristics sensitively. The MWFs applied on the leads and gate induce novel photon-assisted tunnelling, strongly associated with the density of states (DOS) of the SWCN leads. The SWCN leads act as quantum wires, and the compound effect induces nonlinear current behavior and resonant tunnelling in a larger region of energy scale. Negative differential conductance (NDC) is clearly observed, as the source-drain junction capacitances C_L, and C_R are large enough. The multi-resonant NDC oscillation appears due to the charging and photon-electron pumping effects associated with the contribution of multi-channel quantum wires.

PACS. 73.40.-c Electronic transport in interface structures – 73.63.Fg Nanotubes – 73.61.Wp Fullerenes and related materials – 73.22.-f Electronic structure of nanoscale materials: clusters, nanoparticles, nanotubes, and nanocrystals

1 Introduction

With the development of nanotechnology, the fabrication of various nano-devices becomes possible, and it stimulates the research activities in the nanometer scale both in theoretical and experimental aspects. The main effect of nano-systems at low temperature is the quantum behavior of the confined electrons. A quantum dot (QD) is one of such devices with three dimensions being confined in the nanometer regime. The electron energy of a QD is discrete, and the density of state (DOS) exhibits distinct difference from other nano-devices. Coherent tunnelling reveals another major behavior of such mesoscopic systems since the sizes of the devices are smaller than the electron coherent length. As a QD is extremely small, the Coulomb interaction is very important, and the charging-discharging behavior results in novel resonant tunnelling phenomena [1–6].

Single-wall carbon nanotubes (SWCNs) are ideal materials and samples for investigation because of their unique features related to electronics, such as the metal-semiconductor transition [7–9]. The quasi-one-dimensional construction exhibits quantization in the transversal direction, while it is continuous in the longitudinal direction. This provides new quantum wires for testing some existing mesoscopic theoretical results. Metallic quantum wires can be employed as the interconnects for future nano-electronics, while the semiconducting SWCNs can be used as the quantum devices. The Schottky barrier in metal-semiconductor junctions [10,11], the diode effect [12] and the field effect transistor [13,14] all make carbon nanotubes (CNs) excellent prospective materials for future electronic devices. Consequently, mesoscopic transport through CN based devices presents a new investigation paradigm [15–18].

Photon-assisted tunnelling has been of recurring interest in the mesoscopic transport regime since the theoretical work of Bruder et al. shown in reference [2]. They derived a non-Markovian master equation to study the nonlinear time-dependent transport in small semiconductor QD. The many-body nonequilibrium distribution functions of the QD have been calculated. By employing Floquet theory [19], the quantum mechanical calculation performed by Holthaus has displayed that the miniband of quasienergies collapses at singular values of the ac fields. Reference [20] has reported an experimental investigation of electrical transport in the sequential resonant tunnelling regime of superlattices submitted to an intense terahertz electric field. They showed that far-infrared radiation introduces new photon-mediated conduction channels in the devices. The scattering-matrix

[a] e-mail: zhaohonk@yahoo.com

approach on phase-coherent transport was generalized to nonlinear ac transport by Pedersen and Büttiker [21]. They presented a theory of photon-assisted electron transport, in which charge and current conservation are satisfied for all Fourier components of the current. The ac Stark effect and photon-assisted mesoscopic transport through toroidal carbon nanotube (TCN) based devices have been investigated by one of the authors et al. in reference [22]. The ac flux enhances the energy gap, and the DOS exhibits photon absorption and emission. The side peaks and current suppressions result from the quantum nature of the TCN and applied MWFs.

In this paper, we investigate a system with an ultrasmall quantum dot connected to two SWCN leads, with the gate capacitively coupled to the QD. The SWCN leads act as quantum wires whose electronic structures make important contributions to the output current-voltage characteristics. The Coulomb interaction and the capacitances of junctions play significant roles in the mesoscopic transport. This system is quite different from the one without Coulomb interaction and the leads being normal metals. Since CNs have special electronic structures, the DOS induces specific effects in the resultant electronic properties. Therefore, the usual wide-band limit method of calculation is invalid. We are interested in the case of double coherent microwave fields applied to the system through its gate and source-drain terminals. The applied ac fields induce charging-discharging procedure, and the capacitances of junctions and QD dominate the actual transport. The information of external MWFs is transferred to the tunnelling current and differential conductance. Nonlinear photon-assisted tunnelling and negative differential conductance (NDC) are clearly exhibited. We employ the nonequilibrium Green's function (NGF) technique to describe the transport formulas. The tight-binding model is employed for calculating electron transport through the CN systems where the Coulomb interaction is neglected [23,24]. The tight-binding calculation is relatively simple compared with the first principles calculation [25]. On the other hand, the theoretical prediction [26,27] of Luttinger liquid behavior in a SWCN at low energy scale has been verified in transport experiments [28]. However, the tight-binding calculation can provide the main properties of CN systems, such as the electron structure, local density of states, and electron transport. Many scanning tunnelling spectroscopic results are fully interpreted in terms of the independent electron model [29]. We use the tight-binding model to describe the electronic properties of the SWCN leads, which can help us understand the main physical feature of the mesoscopic transport problem. Section 2 addresses the model formalism and current formula derivation. Section 3 is devoted to the numerical calculation and result analysis. Brief concluding remarks are presented in the last section.

2 Model and formalism

Our system is composed of three parts: the ultra-small QD being coupled to two SWCN leads by tunnelling junctions with capacitances C_L and C_R. A metallic gate is contacted to the central QD with capacitance C_g. The SWCN leads act as equilibrium reservoirs which satisfy the grand canonical ensembles. External MWFs are applied to the two leads and the gate. The external potential differences induced by the MWFs are expressed by different angular frequencies ω_j. The energy spectra of the two leads are modified as $\varepsilon_{\delta\gamma,k\sigma}(t) = \varepsilon^0_{\delta\gamma,k\sigma} + \sum_{j=1}^{2} \Delta_{\gamma_j} \cos\omega_j t$, for $\gamma \in \{L, R\}$, where $\varepsilon^0_{\delta\gamma,k\sigma}$ are the isolated energy of CN leads. The gate potential is determined by the time-dependent potential as $eV_g(t) = \mu_g + \sum_{j=1}^{2} \Delta_{g_j} \cos\omega_j t$, where μ_g is the chemical potential of gate in the absence of external field. The total Hamiltonian is therefore given by the summation of the sub-Hamiltonians of the two leads, the QD, and tunnelling terms as

$$H(t) = \sum_{\delta\gamma k\sigma} \varepsilon_{\delta\gamma,k\sigma}(t) c^\dagger_{\delta\gamma,k\sigma} c_{\delta\gamma,k\sigma} + \sum_{\ell\sigma} E_{\ell\sigma} n_{\ell\sigma} + E_c \sum_{\ell\sigma} n_{\ell\sigma}[n_{\ell\bar{\sigma}} + 2n_0(t)] + \sum_{\delta\gamma k\ell\sigma} \Big[R_\gamma c^\dagger_{\delta\gamma,k\sigma} d_{\ell\sigma} + \text{h.c.} \Big], \quad (1)$$

where $n_{\ell\sigma} = d^\dagger_{\ell\sigma} d_{\ell\sigma}$. The operators $c^\dagger_{\delta\gamma,k\sigma}(c_{\delta\gamma,k\sigma})$, and $d^\dagger_{\ell\sigma}(d_{\ell\sigma})$ are the creation (annihilation) operators of electron in the two leads and the central QD, respectively. The spin subscript σ in the Hamiltonian takes the value $\sigma = \pm 1$, which denotes the situation for spin-up $\uparrow$, and spin-down $\downarrow$. R_γ is the interaction strength of electrons between the γth lead and the central QD. The ultrasmall QD is approximated by the Coulomb-blockade model [30], which is somewhat like the Anderson model. $E_c = e^2/2C$ is the charging energy with $C = \sum_{i=L,R,g} C_i$. In the Hamiltonian (1), $en_0(t) = \sum_{i=L,R,g} C_i V_i(t)$ is related to the polarization charges produced by the time-dependent voltages of the left and right leads $eV_\gamma(t) = \mu_\gamma + \sum_{j=1}^{2} \Delta_{\gamma_j} \cos\omega_j t$, as well as the time-dependent gate voltage $eV_g(t)$ applied to the QD through the capacitance C_g. This model is used by Bruder and Schoeller to investigate the charging effects in the ultrasmall QD coupled to normal metal leads [2]. The difference of our system is that the ultrasmall QD is coupled to metallic SWCN leads. We take the chemical potential of the right lead as the reference of energy measurement.

In order to handle the problem conveniently, we make the gauge transformation $\Psi(t) = \hat{U}(t)\tilde{\Psi}(t)$ in the Schrödinger equation, where the unitary operator is defined by

$$\hat{U}(t) = \exp\left\{ -\frac{i}{\hbar} \sum_{j=1}^{2} \left[\sum_{\delta\gamma k\sigma} \left(\Delta_{\gamma_j}/\omega_j \right) c^\dagger_{\delta\gamma,k\sigma} c_{\delta\gamma,k\sigma} + \sum_{\ell\sigma} \left(\tilde{\Delta}_j/\omega_j \right) d^\dagger_{\ell\sigma} d_{\ell\sigma} \right] \sin\omega_j t \right\}. \quad (2)$$

In the unitary operator, we have defined the relation $\tilde{\Delta}_j = \sum_{i=L,R,g} C_i \Delta_{ij}/C$ for writing the formula more concisely.

The Hamiltonian of the system is transformed to the new form after the gauge transformation

$$\begin{aligned}\bar{H}(t) = &\sum_{\delta\gamma k\sigma} \varepsilon^0_{\delta\gamma,k\sigma} c^\dagger_{\delta\gamma,k\sigma} c_{\delta\gamma,k\sigma} + \sum_{\ell\sigma} E_{\ell\sigma} n_{\ell\sigma} \\ &+ E_c \sum_{\ell\sigma} n_{\ell\sigma} \left(n_{\ell\bar{\sigma}} + \frac{2}{e^2} \sum_{i=L,R,g} C_i \mu_i \right) \\ &+ \sum_{\delta\gamma k\ell\sigma} \left[\bar{R}_\gamma(t) c^\dagger_{\delta\gamma,k\sigma} d_{\ell\sigma} + \text{h.c.} \right]. \end{aligned} \tag{3}$$

Through the transformation, the time-dependent energies in the subsystems become time-independent ones, while the interaction strength R_γ is transformed to the time-dependent one

$$\bar{R}_\gamma(t) = R_\gamma \exp\left\{ \frac{i}{\hbar} \sum_{j=1}^{2} \left[\left(\Delta_{\gamma_j} - \tilde{\Delta}_j \right) / \omega_j \right] \sin \omega_j t \right\}.$$

The tunnelling current can be derived by employing the NGF technique, the continuity equation and Heisenberg equation. Following the approach of Jauho, Wingreen, and Meir, we can express the tunnelling current by the Green's functions of QD $G^X_{\ell\sigma,\ell'\sigma'}(t,t')$, $(X \in \{r,a,<\})$. The time-dependent tunnelling current in the left lead is determined by the formula [31]

$$\begin{aligned} I_L = -\frac{2e}{\hbar} \int_{-\infty}^{t} dt_1 \int \frac{d\epsilon}{2\pi} \text{Im} \Bigg\{ &\sum_{\ell\ell'\sigma\sigma'} \Gamma^L_\sigma(\epsilon, t_1, t) e^{-\frac{i}{\hbar}\epsilon(t_1 - t)} \\ &\times \left[G^r_{\ell\sigma,\ell'\sigma'}(t,t_1) f_L(\epsilon) + G^<_{\ell\sigma,\ell'\sigma'}(t,t_1) \right] \Bigg\}, \end{aligned} \tag{4}$$

where we have denoted the quantity $\Gamma^\gamma_\sigma(\epsilon,t_1,t) = 2\pi\rho_{\gamma\sigma}(\epsilon)\bar{R}_\gamma(t)\bar{R}^*_\gamma(t_1)$. The DOS of the γth CN lead is defined by $\rho_{\gamma\sigma}(\epsilon) = \sum_{k\delta} \delta(\epsilon - \varepsilon^0_{\delta\gamma,k\sigma})$. In deriving the tunnelling current formula, the Green's function of isolated CN lead

$$g^{r(a)}_{\delta\gamma,k\sigma}(t_1,t_2) = \mp \frac{i}{\hbar} \theta(\pm t_1 \mp t_2) \exp\left[-\frac{i}{\hbar} \varepsilon^0_{\delta\gamma,k\sigma}(t_1 - t_2) \right]$$

is employed for describing the self-energies of the leads. The DOS can be determined by the Fourier transformed Green's function of isolated CN lead as $\rho_{\gamma\sigma}(\epsilon) = -\sum_{k\delta} Im g^r_{\delta\gamma,k\sigma}(\epsilon)/\pi$, where $g^r_{\delta\gamma,k\sigma}(\epsilon) = 1/(\epsilon - \varepsilon^0_{\delta\gamma,k\sigma} + i\eta)$.

We employ the equation of motion method to derive the Green's function [32]. The retarded Green's function of the isolated QD is defined as

$$g^r_{\ell\sigma,\ell'\sigma'}(t,t') = -\frac{i}{\hbar}\theta(t-t') \exp\left[-\frac{i}{\hbar} \xi_{\ell\sigma}(t-t') \right] \delta_{\ell\ell'}\delta_{\sigma\sigma'},$$

where $\xi_{\ell\sigma} = E_{\ell\sigma} + \sum_{i=L,R,g} C_i\mu_i/C$. The Green's function of the coupled QD can be derived from the Dyson-like equation

$$\begin{aligned} G^r_{\ell\sigma,\ell'\sigma'}(t,t') = &\int dt_1 g^r_{\ell\sigma,\ell\sigma}(t,t_1) \tilde{g}^r_{\ell\sigma,\ell'\sigma'}(t_1,t') \\ &+ \sum_{\ell''} \iint dt_1 dt_2 g^r_{\ell\sigma,\ell\sigma}(t,t_1) \tilde{\Sigma}^r_{\ell\sigma}(t_1,t_2) \\ &\times G^r_{\ell''\sigma,\ell'\sigma'}(t_2,t') + g^r_{\ell\sigma,\ell'\sigma'}(t,t'). \end{aligned} \tag{5}$$

In the Dyson-like equation above we have defined the Green's function

$$\begin{aligned} \tilde{g}^r_{\ell\sigma,\ell'\sigma'}(t,t') = &-\frac{i}{\hbar}\theta(t-t') \exp\left[-\frac{i}{\hbar}(\xi_{\ell\sigma} + 2E_c)(t-t') \right] \\ &\times 2E_c \langle n_{\ell\bar{\sigma}} \rangle \delta_{\ell\ell'}\delta_{\sigma\sigma'}, \end{aligned}$$

where the charging energy E_c and occupation number of electron in the QD $\langle n_{\ell\bar{\sigma}} \rangle$ are involved. The self-energy of the system is defined as

$$\begin{aligned} &\tilde{\Sigma}^X_{\ell\sigma}(t,t') = \\ &\qquad \sum_\gamma \left[\Sigma^X_{\gamma\sigma}(t,t') + \int dt_1 \tilde{g}^r_{\ell\sigma,\ell\sigma}(t,t_1) \Sigma^X_{\gamma\sigma}(t_1,t') \right], \end{aligned}$$

in which the contribution of Coulomb interaction is included. In the derivation of equation (5), the mean-field approximation is used to truncate the equation chain in order to obtain the closed solution [32]. The self-energy $\Sigma^X_{\gamma\sigma}(t,t') = \sum_{\delta k} \bar{R}^*_\gamma(t) g^X_{\delta\gamma,k\sigma}(t,t') \bar{R}_\gamma(t')$, with $X \in \{r,a,<\}$, represents the interaction of the leads with the QD. Similarly, the Keldysh Green's function can be derived from the integral equation

$$\begin{aligned} G^<_{\ell\sigma,\ell'\sigma'}(t,t') = &\sum_{\ell''} \iint dt_1 dt_2 g^r_{\ell\sigma,\ell\sigma}(t,t_1) \\ &\times \Big[\tilde{\Sigma}^r_{\ell\sigma}(t_1,t_2) G^<_{\ell''\sigma,\ell'\sigma'}(t_2,t') \\ &+ \tilde{\Sigma}^<_{\ell\sigma}(t_1,t_2) G^a_{\ell''\sigma,\ell'\sigma'}(t_2,t') \Big]. \end{aligned} \tag{6}$$

In the Keldysh self-energy $\tilde{\Sigma}^<_{\ell\sigma}(t_1,t_2)$, the Keldysh Green's function of the γth CN lead is given by

$$g^<_{\delta\gamma,k\sigma}(t,t') = \frac{i}{\hbar} f\left(\varepsilon^0_{\delta\gamma,k\sigma} \right) \exp\left[-\frac{i}{\hbar} \varepsilon^0_{\delta\gamma,k\sigma}(t-t') \right],$$

where $f(\varepsilon^0_{\delta\gamma,k\sigma})$ is the Fermi distribution function of the γth lead defined as $f_\gamma(\epsilon) = 1/\{\exp[(\epsilon - \mu_\gamma)/K_BT] + 1\}$. The Green's functions of the coupled QD can be obtained by solving equations (5) and (6). Performing the Fourier transformation over equation (5), one can find the retarded Green's function of coupled QD as

$$G^r_{\ell\sigma,\ell'\sigma'}(\epsilon) = \frac{g^r_{\ell\sigma}(\epsilon) \left[1 + 2E_c \langle n_{\ell\bar{\sigma}} \rangle g^r_{\ell\sigma}(\tilde{\epsilon}) \right] \delta_{\ell\ell'}\delta_{\sigma\sigma'}}{1 - g^r_{\ell\sigma}(\epsilon) \left[1 + 2E_c \langle n_{\ell\bar{\sigma}} \rangle g^r_{\ell\sigma}(\tilde{\epsilon}) \right] \tilde{\Sigma}^r(\epsilon)}, \tag{7}$$

where $\tilde{\epsilon} = \epsilon - 2E_c$. The Fourier transformed self-energy $\tilde{\Sigma}^r(\epsilon)$ is determined by

$$\begin{aligned} \tilde{\Sigma}^r(\epsilon) = &\sum_{\delta\gamma k} \sum_{p_1,p_2,p_3} |R_\gamma|^2 J_{p_1}(\Lambda_1) J_{p_2}(\Lambda_2) J_{p_3}(\Lambda_1) \\ &\times J_{p_2+(p_1-p_3)q}(\Lambda_2) g^r_{\delta\gamma,k\sigma}\left(\epsilon - p_1\hbar\omega_1 - p_2\hbar\omega_2 \right), \end{aligned}$$

where $q = \omega_1/\omega_2$, and $g^r_{\ell\sigma}(\epsilon) = 1/(\epsilon - \xi_{\ell\sigma} + i\eta)$ is the Fourier transformation of the isolated QD. We have employed the property of a Bessel function $\exp(i\Lambda_j \sin\omega t) = \sum_p J_p(\Lambda_j)\exp(ip\omega t)$, where Λ_j is the magnitude difference of the ac fields defined by $\Lambda_j = (\Delta_{\gamma_j} - \tilde{\Delta}_j)/\hbar\omega_j$, $(j = 1, 2)$. The Keldysh Green's function can be derived similarly to be expressed as the product of the retarded and advanced Green's functions of the QD

$$G^<_{\ell\sigma,\ell\sigma}(\epsilon) = i \sum_{p_1,p_2,p_3} \sum_{\gamma} \tilde{\Gamma}^{\gamma}_{p_1,p_2,p_3}(\epsilon)|G^r_{\ell\sigma,\ell\sigma}(\epsilon)|^2 \times f_\gamma\left(\epsilon - p_1\hbar\omega_1 - p_2\hbar\omega_2\right). \quad (8)$$

In the above formula, we have denoted the line-width function of the γth lead in the presence of ac fields as

$$\tilde{\Gamma}^{\gamma}_{p_1,p_2,p_3}(\epsilon) = \Gamma^{\gamma}_{\sigma}\left(\epsilon - p_1\hbar\omega_1 - p_2\hbar\omega_2\right) J_{p_1}(\Lambda_1) \times J_{p_2}(\Lambda_2) J_{p_3}(\Lambda_1) J_{p_2+(p_1-p_3)q}(\Lambda_2),$$

where $\Gamma^{\gamma}_{\sigma}(\epsilon)$ is the line-width of the γth lead in the absence of ac fields defined by $\Gamma^{\gamma}_{\sigma}(\epsilon) = 2\pi\rho_{\gamma\sigma}(\epsilon)|R_\gamma|^2$. The occupation number has to be calculated through the equation self-consistently

$$\langle n_{\ell\sigma}\rangle = \frac{1}{2\pi}\mathrm{Im}\int d\epsilon G^<_{\ell\sigma,\ell\sigma}(\epsilon). \quad (9)$$

Taking a time-average over the tunnelling current formula (4), we can obtain the tunnelling current through the QD by substituting the Green's functions given in equations (7) and (8)

$$I = \frac{e}{h}\sum_{\ell\sigma}\sum_{p_1,p_2,p_3}\sum_{p'_1,p'_2,p'_3}\int d\epsilon \tilde{\Gamma}^{L}_{p_1,p_2,p_3}(\epsilon)\tilde{\Gamma}^{R}_{p'_1,p'_2,p'_3}(\epsilon) \times |G^r_{\ell\sigma,\ell\sigma}(\epsilon)|^2 \left[f_L\left(\epsilon - p_1\hbar\omega_1 - p_2\hbar\omega_2\right) - f_R\left(\epsilon - p'_1\hbar\omega_1 - p'_2\hbar\omega_2\right)\right]. \quad (10)$$

Due to the current conservation, the magnitudes of the tunnelling current in different parts are equal, i.e., $I = I_L$. This is the Landauer-Büttiker-like formula in the presence of external ac fields [32]. Equation (10) contains all the mesoscopic transport information of the system. The detailed tunnelling feature is determined by the structure of QD, the charging energy E_c, the structures of the CN leads, the junction capacitances C_L, C_R and C_g, the source-drain bias and gate voltage, the external MWFs and the coupling strengths. The temperature dependence is associated with the Fermi distribution function. We assume the junction capacitances are known, as is treated in references [2] and [6]. The Green's functions involve the occupation number $\langle n_{\ell\sigma}\rangle$, so that we solve the Green's function self-consistently. As $\Lambda_j = 0$, the tunnelling current (10) reduces to the Landauer-Büttiker-like formula [33] in the absence of the external MWFs. The interaction strengths of the external MWFs Λ_j are determined directly by their magnitudes of potential differences and frequencies. The mesoscopic transport is similar to the situation in the absence of external MWFs when $\Delta_{\gamma_j} = \tilde{\Delta}_j$, even if each of the external fields is not zero. The resonant peaks of the QD without connecting to CN leads are located at $\epsilon = \xi_{\ell\sigma} + p_1\hbar\omega_1 + p_2\hbar\omega_2$, and $\epsilon = \xi_{\ell\sigma} + 2E_c + p_1\hbar\omega_1 + p_2\hbar\omega_2$, $(p_1, p_2 = 0, 1, 2, ...)$. However, as the QD is connected to the CN leads, new resonant peaks arise due to the influences of the quantum wires.

3 Numerical calculation

In this section, we perform the numerical calculation on the tunnelling current and differential conductance of the system at zero temperature. Armchair CNs are chosen as the leads for connecting the QD. This kind of material possesses metallic properties, and it acts as a good conductor for electron transport. Similar behavior is also displayed in the other metallic zigzag CN leads. In the tight-binding approximation, the energy of armchair (n,n) CN can be derived as [34]

$$\varepsilon^{(0)}_{\delta\gamma,k\sigma} = \delta\gamma_0\left\{1 + 4\cos\left(\frac{ak_y}{2}\right)\cos\left(\frac{\sqrt{3}ak_x}{2}\right) + 4\cos^2\left(\frac{ak_y}{2}\right)\right\}^{\frac{1}{2}}, \quad (11)$$

where $\sqrt{3}ak_x/2 = \pi q/n$, $q = 1, 2, \ldots, 2n$, $\delta = \pm$, and $\gamma_0 = 3.033$ eV. The energy in the transversal direction is quantized, while in the longitudinal direction it is not restricted. As the electrodes are connected to the QD, the tunneling current is formed by applying different chemical potentials to the leads. Without loss of generality, we only present the calculation for the single-level QD by setting $E_{\ell\sigma} = 0$ for simplification. At zero temperature the current formula (10) is reduced to

$$I = \frac{e}{h}\sum_{\ell\sigma}\sum_{p_1,p_2,p_3}\sum_{p'_1,p'_2,p'_3}\int_{p'_1\hbar\omega_1+p'_2\hbar\omega_2}^{eV+p_1\hbar\omega_1+p_2\hbar\omega_2} d\epsilon \times \tilde{\Gamma}^{L}_{p_1,p_2,p_3}(\epsilon)\tilde{\Gamma}^{R}_{p'_1,p'_2,p'_3}(\epsilon)|G^r_{\ell\sigma,\ell\sigma}(\epsilon)|^2, \quad (12)$$

where we have set the chemical potential of the right lead at zero. The concrete structure of QD possesses specific charging energy which denotes the interaction strength of electrons in the QD. We choose the charging energy to be $E_c = 3.125$ meV, which is in the same order of the experimentally observed value in reference [35]. For the weakly coupled system, the coupling strengthens between the two armchair CN leads and QD are chosen as $|R_L| = |R_R| = 24.5$ meV. We consider the situation that the double coherent external MWFs are located in the frequency region 10^{11} Hz, which can be achieved experimentally. In particular, we consider the fields with the frequency 4.78×10^{11} Hz, whose photon energies are $\hbar\omega_1 = \hbar\omega_2 = 2.0$ meV. The transport features change sensitively with respect to the ratio of C_L, C_R and C_g to the total capacitance C. We perform the numerical calculations to show the $I - V$ characteristics, differential conductance, and the current versus gate voltage for the two

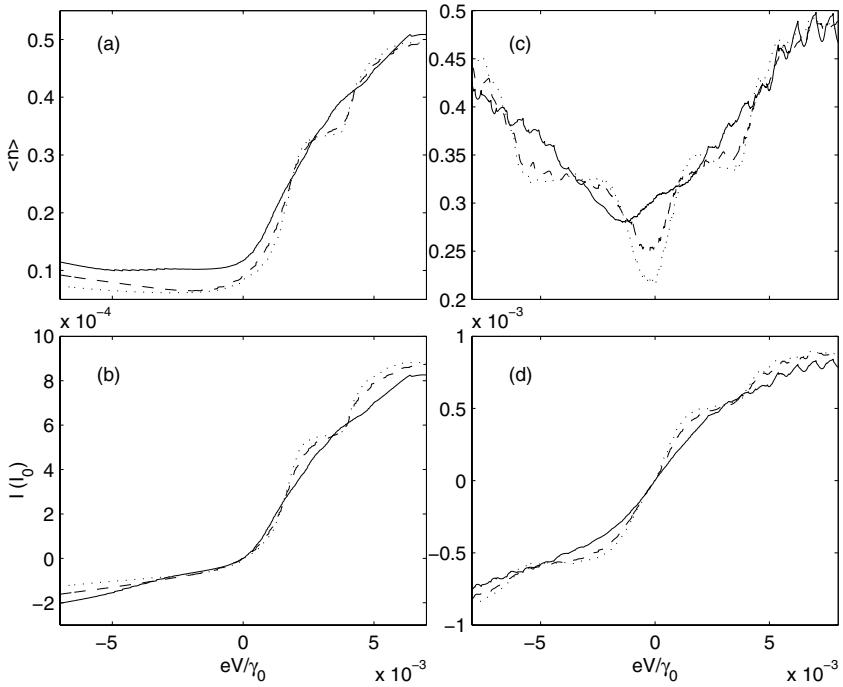

Fig. 1. The occupation number $\langle n\rangle$ and current I versus source-drain bias V as $eV_g = 0.002\gamma_0$. Diagrams (a), (b) correspond to $R = 0.1$, while diagrams (c), (d) correspond to $R = 0.4$, respectively. The dotted, dashed and solid curves are associated with (1) $\Lambda_1 = \Lambda_2 = 0$; (2) $\Lambda_1 = 0$,$\Lambda_2 = 0.8$; and (3) $\Lambda_1 = \Lambda_2 = 0.8$, respectively.

cases as $C_L/C = C_R/C = 0.1$ and $C_L/C = C_R/C = 0.4$ separately. We take γ_0 as the energy scale for all of the energy quantities. The conductance is scaled by $G_0 = 2e^2/h$, and the current is scaled by $I_0 = 2e\gamma_0/h$. The CN leads are chosen as the armchair (9,9) SWCNs, whose DOS structure can be found in reference [34].

3.1 The case of $C_L/C = C_R/C = 0.1$

In this subsection, we discuss the transport properties for the case when $R = C_L/C = C_R/C = 0.1$. In Figures 1a and b, we display the occupation number of electron $\langle n\rangle$ and $I-V$ characteristics versus the source-drain bias eV as $eV_g = 0.002\gamma_0$, respectively. The dotted, dashed and solid curves are associated with the system in the absence, in the presence of single, and double MWFs. When there is no external MWFs, the occupation number $\langle n\rangle$ increases with respect to the voltage to the saturate value $\langle n\rangle \approx 0.48$. An obvious step emerges as the source-drain bias increases to $eV \approx 2E_c$, which is the Coulomb-blockade effect. When double MWFs are applied to the system, the occupation number shifts. As eV is positively large enough, the larger saturate value 0.5 (solid curve) is reached compared with the case as $\Lambda_j = 0$. However, the applied MWFs smear the step of occupation number at $eV \approx 2E_c$. We present the $I-V$ characteristics of the case in diagram (b). Similar to the occupation number shown in (a), the main step located at $eV \approx 2E_c$ is observed in the absence of MWFs (dotted curve). This signifies that a new channel is open at $eV \approx 2E_c$ for electrons to transport through. This channel originates from the Coulomb interaction. As the QD is large, the charging energy is small enough to be neglected, and hence this channel disappears. As the MWFs are applied to the system, one observes that the main step caused by the charging energy is smeared. The contribution of a single applied field is observed to be located in the intermediate of the two cases with $\Lambda_j = 0$ and $\Lambda_j = 0.8$, $(j = 1, 2)$. The smearing of the Coulomb-blockade step by the applied double MWFs is associated with the photon-electron pumping effect. As the source-drain bias is located at the Coulomb-blockade region, the charging energy acts as a threshold to resist the electron tunnelling. The applied double MWFs provide enough energy for electrons to overcome the threshold.

Figure 2 shows the differential conductance dI/dV versus eV as $\Lambda_j = 0$ and $\Lambda_j = 0.8$, $(j = 1, 2)$, respectively. The diagrams (a) and (b) are related to the case as $R = 0.1$. In the absence of MWFs, the differential conductance displays two cluster resonances as shown in diagram (a). These cluster resonances are associated with the abrupt changes around the current step. The resonant peaks of the differential conductance also reveal the channels of CN quantum wires. The maximum differential conductance is near G_0, which indicates ideal channel conductance. When the double MWFs are applied, the photon-assisted tunnelling is strongly dependent on the magnitude of the applied fields Λ_j as shown in diagram (b). The resonant peaks are split further, and the magnitude of differential conductance is reduced. The novel peaks in the dI/dV curve are associated with the mini steps and side-band induced by the MWFs in solid curve of Figure 1b. The resonant peaks display novel channels for electrons to tunnel in a wider region of voltage. The negative differential conductance (NDC) emerges

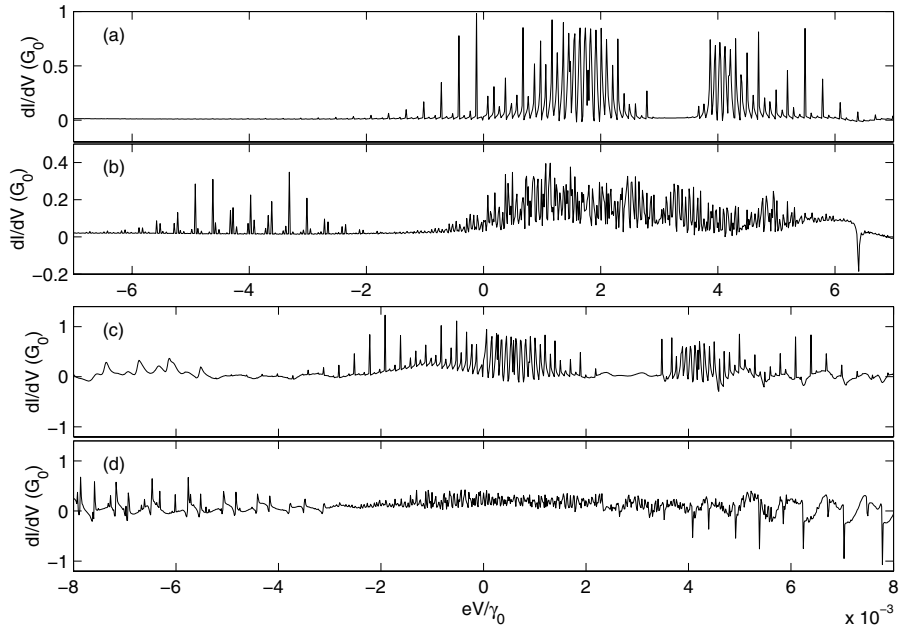

Fig. 2. The differential conductance dI/dV versus the source-drain bias eV as $eV_g = 0.002\gamma_0$. The curves of dI/dV for $R = 0.1$ corresponding to $\Lambda_1 = \Lambda_2 = 0$ and $\Lambda_1 = \Lambda_2 = 0.8$ are shown in diagrams (a) and (b). The curves of dI/dV for $R = 0.4$ corresponding to $\Lambda_1 = \Lambda_2 = 0$ and $\Lambda_1 = \Lambda_2 = 0.8$ are shown in diagrams (c) and (d).

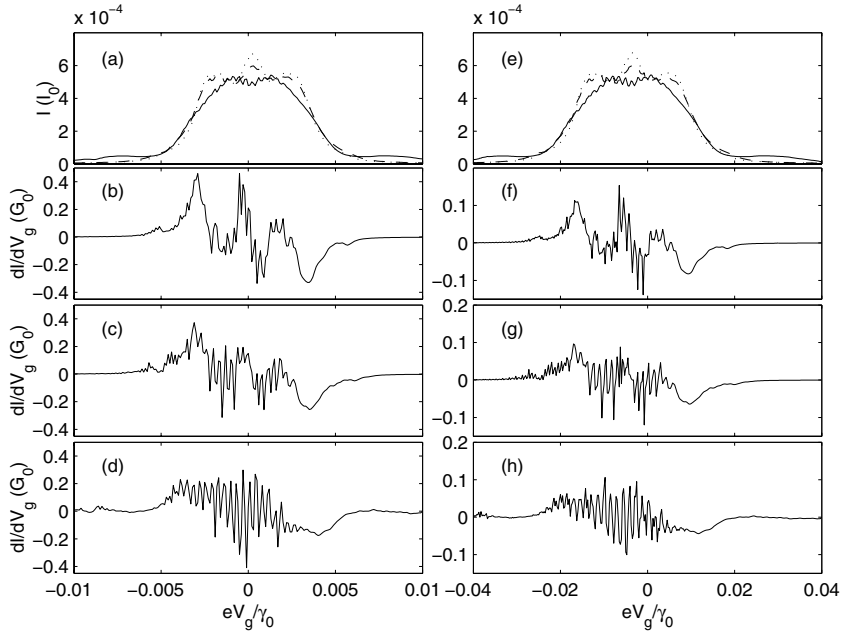

Fig. 3. The current I and differential conductance dI/dV versus the gate voltage V_g as $eV = 0.003\gamma_0$. Diagrams (a), (b), (c) and (d) are associated with the case for $R = 0.1$, while diagrams (e), (f), (g) and (h) are associated with the case for $R = 0.4$. In diagrams (a) and (e), the dotted, dashed and solid curves correspond to (1) $\Lambda_1 = \Lambda_2 = 0$; (2) $\Lambda_1 = 0$, $\Lambda_2 = 0.8$; and (3) $\Lambda_1 = \Lambda_2 = 0.8$, respectively. The diagrams (b) and (f) correspond to $\Lambda_1 = \Lambda_2 = 0$; (c), (g) correspond to $\Lambda_1 = 0$, $\Lambda_2 = 0.8$; (d), (h) correspond to $\Lambda_1 = \Lambda_2 = 0.8$, respectively.

at $eV = 0.0064\gamma_0$, and arises from the photon-electron pumping effect in the capacitively coupled system.

The tunnelling current versus gate voltage is illustrated in Figure 3a as $eV = 0.003\gamma_0$. In the absence of external MWFs, there exist three peaks located on the current plateau. The central peak is higher than the side peaks. The side peaks arise from the charging energy. The peaks are suppressed and smeared by applying the double external MWFs. Some small resonant peaks appear due to the splitting of the original peaks on the current plateau. The influence of single MWF applied to the system is also presented for comparison. The splitting and smear of resonant peaks of current versus gate voltage can be displayed explicitly by the curves of dI/dV_g shown in diagrams (b), (c) and (d) of Figure 3. The fierce variations of dI/dV_g correspond to the resonant peaks and valleys of

$I - V_g$ curves in diagram (a). The suppression and smear of the resonant peaks of current in diagram (a) can be understood as the external MWFs splitting the original current peaks, and the heights of peaks are suppressed correspondingly. Since the splitting causes the side peaks to form side multi-peaks, the split peaks combine with the original ones to form a new configuration of current resonance. The contribution of the multi-channel CN leads is contained in the rapid vibration of dI/dV_g. We observe that there exists distinctly different influences on the mesoscopic transport between the single MWF and double MWFs applied CN-QD system.

3.2 The case of $C_L/C = C_R/C = 0.4$

In this subsection, we investigate the case when $R = C_L/C = C_R/C = 0.4$. The occupation number and current versus source-drain bias eV are shown in Figures 1c, and d as $eV_g = 0.002\gamma_0$. Compared with the case discussed in the subsection A as $R = 0.1$, one observes that the transport behavior is quite different between the two cases as $R = 0.4$ and $R = 0.1$. The occupation number decreases to its minimum value and then increases to reach its saturation value as the source-drain bias eV varies from the negative region to the positive region. There are several steps in the occupation number as the MWFs are removed. The main steps are associated with the charging energy E_c. The capacitances of the junctions have a major effect on the new configuration of occupation number. As the external MWFs are applied to the system, the current is modified by introducing new steps and peaks. The valley of the $\langle n \rangle$ curve is elevated much higher by the external fields. Correspondingly, the $I - V$ characteristics are strongly modified due to the applied MWFs in this case. The small steps on the right side of the curve change to small peaks on the curve, and the main steps are smeared shown in diagram (d). Obviously, the $I - V$ characteristics are quite different from the one shown in subsection A. This signifies that as the junction capacitances are large enough, the charging effect can cause novel tunnelling behavior.

The differential conductance versus source-drain bias is shown in Figures 2c and d associated with $\Lambda_j = 0$ and $\Lambda_j = 0.8$, $(j = 1, 2)$, respectively. As the magnitude of voltage V is large, new resonant peaks and NDC appear. This indicates that the junction capacitances take important roles in the conduction. The charging effect causes electrons to pile in the junctions, and the source-drain bias is involved in the tunnelling coefficient. When the MWFs are applied, the resonant peaks are split further to form new configurations of differential conductance. The central region of the conductance is suppressed, however, many significant NDC resonant peaks and valleys are produced as the magnitude of source-drain bias is large. The NDC appears in both the positive and negative regimes of eV. Compared with the situation of $R = 0.1$, the case of $R = 0.4$ contains multi-resonances of NDC. The experimental observation of NDC in boron-exposed silicon diode was reported by Lyo and Avouris [36], where single-resonance of NDC is displayed. NDC is the essential property for allowing fast switching in certain types of electronic devices.

The current and differential conductance versus gate voltage are exhibited in Figures 3e, f, g and h as $eV = 0.003\gamma_0$. The peaks of resonant tunnelling current appear with similar forms as those in the case when $R = 0.1$, but the main resonant peak of the case $R = 0.4$ is much wider than that of the case $R = 0.1$. This implies that by increasing the capacitance ratio R, one can obtain wide-band resonant tunnelling current. The curves of dI/dV_g shown in f, g and h possess some similarities as the case for $R = 0.1$. One can find the non-trivial differences of the dI/dV_g curves from the two cases. The increasing of capacitance ratio corresponds to stretch the differential conductance region with respect to eV_g. The differential conductance oscillation is also suppressed due to increasing the ratio R. The multi-resonance of the differential conductance versus gate voltage implies the contribution of multi-channel quantum wires of the leads and the applied MWFs.

4 Concluding remarks

We have investigated the mesoscopic transport through the system with an ultrasmall QD coupled to two CN leads. The CN leads act as quantum wires which provide multi-channels for electron to tunnel. The specific DOS structures of CN leads play important roles in the tunnelling behavior. The restriction of electrons in quasi-one-dimensional region causes the quantization of electron energy in the transversal direction of movement. The usual wide-band limit approximation in numerical calculation is invalid, and the contribution of multi-channel quantum wires results in novel resonant transport behaviors. The output characteristics depend sensitively on the charging energy in the central QD, and the junction capacitances C_L, C_R and C_g. A new channel is opened near $eV \approx 2E_c$ originating from the Coulomb interaction for electrons to transport through. Photon-assisted tunnelling is strongly dependent on the magnitude of the applied fields. The current resonant peaks are suppressed and smeared to form new appearance by applying external MWFs. The applied double MWFs on the leads and gate can smear the current step caused by the charging energy E_c. This current smear by the ac fields can be attributed to the photon-electron pumping effect. The NDC appears due to the photon-electron pumping effect associated with the charging-discharging of electrons in the capacitively connected QD system. This effect is enhanced by increasing the capacitance ratio $C_L/C = C_R/C$. Therefore, we can adjust the parameters such as terminal bias eV, gate voltage V_g, the capacitance ratio, and external MWFs to obtain desired tunnelling characteristics of the definite CN-QD system.

This work was supported by the National Natural Science Foundation of China under the Grant No. 10375007, the Project-sponsored by SRF for ROCS, SEM, and by a RGC grant from the SAR Government of Hong Kong under Grant No. HKU 7032/03P.

References

1. *Single Charge Tunneling*, edited by H. Grabert, M. Devoret, NATO ASI Ser. B, Vol. **294** (Plenum, New York, 1991)
2. C. Bruder, H. Schoeller, Phys. Rev. Lett. **72**, 1076 (1994); C. Bruder, R. Fazio, H. Schoeller, Phys. Rev. Lett. **76**, 114 (1996)
3. C.A. Stafford, Phys. Rev. Lett. **77**, 2770 (1996)
4. M.A. Kastner, Rev. Mod. Phys. **64**, 849 (1992)
5. Y. Meir, N.S. Wingreen, P.A. Lee, Phys. Rev. Lett. **66**, 3048 (1991)
6. M. Büttiker, C.A. Stafford, Phys. Rev. Lett. **76**, 495 (1996)
7. S. Iijima, Nature (London) **354**, 56 (1991)
8. D.S. Bethune, C.H. Klang, M.S. de Vries, G. Gorman, R. Savoy, J. Vazquez, R. Beyers, Nature (London) **363**, 605 (1993)
9. S.J. Tans, M.H. Devoret, H. Dai, A. Thess, R.E. Smalley, L.J. Geerligs, C. Dekker, Nature (London) **386**, 474 (1997)
10. S. Heinze, J. Tersoff, R. Martel, V. Derycke, J. Appenzeller, Ph. Avouris, Phys. Rev. Lett. **89**, 106801 (2002)
11. A.A. Odintsov, Phys. Rev. Lett. **85**, 150 (2000)
12. Z. Yao, H.W. Ch. Postma, L. Balents, C. Dekker, Nature (London) **402**, 273 (1999)
13. S.J. Tans, A.R.M. Verschueren, C. Dekker, Nature (London) **393**, 49 (1998)
14. R. Martel, T. Schmidt, H.R. Shea, T. Hertel, Ph. Avouris, Appl. Phys. Lett. **73**, 2447 (1998)
15. Y. Xue, S. Datta, Phys. Rev. Lett. **83**, 4844 (1999); S. Roche, R. Saitio, Phys. Rev. Lett. **87**, 246803 (2001)
16. H. Mehrez, J. Taylor, H. Guo, J. Wang, C. Roland, Phys. Rev. Lett. **84**, 2682 (2000)
17. J. Kong, E. Yenilmez, T.W. Tombler, W. Kim, H. Dai, Phys. Rev. Lett. **87**, 106801 (2001)
18. F. Léonard, J. Tersoff, Phys. Rev. Lett. **83**, 5174 (1999)
19. M. Holthaus, Phys. Rev. Lett. **69**, 351 (1992)
20. P.S.S. Guimarães et al., Phys. Rev. Lett. **70**, 3792 (1993)
21. M.H. Pedersen, M. Büttiker, Phys. Rev. B **58**, 12993 (1998)
22. H.K. Zhao, Eur. Phys. J. B **33**, 365 (2003); H.K. Zhao, J. Wang, Phys. Lett. A **325**, 407 (2004); H.K. Zhao, J. Wang, Eur. Phys. J. B **40**, 93 (2004)
23. X. Blase, L.X. Benedict, E.L. Shirley, S.G. Louie, Phys. Rev. Lett. **72**, 1878 (1994); Yu.A. Krotov, D.H. Lee, S.G. Louie, Phys. Rev. Lett. **78**, 4245 (1997)
24. M. Buongiorno Nardelli, Phys. Rev. B **60**, 7828 (1999); D. Orlikowski et al., Phys. Rev. B **63**, 155412 (2001)
25. J. Taylor, H. Guo, J. Wang, Phys. Rev. B **63**, 245407 (2001)
26. R. Egger, A.O. Gogolin, Phys. Rev. Lett. **79**, 5082 (1997); R. Egger, Phys. Rev. Lett. **83**, 5547 (1999)
27. C.L. Kane, L. Balents, M.P.A. Fisher, Phys. Rev. Lett. **79**, 5086 (1997)
28. M. Bockrath, D.H. Cobden, J. Lu, A.G. Rinzler, R.E. Smalley, L. Balents, P.L. McEuen, Nature (London) **397**, 598 (1999)
29. T.W. Odom, J.L. Huang, P. Kim, C.M. Lieber, J. Phys. Chem. B **104**, 2794 (2000)
30. L.I. Glazman, K.A. Mateev, Zh. Eksp. Teor. Fiz. **98**, 1834 (1990) [Sov. Phys. JETP **71**, 1031 (1990)]
31. A.P. Jauho, N.S. Wingreen, Y. Meir, Phys. Rev. B **50**, 5528 (1994)
32. H.K. Zhao, Phys. Lett. A **226**, 105 (1997); H.K. Zhao, Z. Phys. B **102**, 415 (1997); H.K. Zhao, G.V. Gehlen, Phys. Rev. B **58**, 13660 (1998)
33. R. Landauer, IBM J. Res. Dev. **1**, 223 (1957); M. Büttiker, Phys. Rev. Lett. **57**, 1761 (1986)
34. R. Saito, G. Dresselhaus, M.S. Dresselhaus, *Physical Properties of Carbon Nanotubes* (Imperial College Press, London, 1998)
35. K. Ishibashi, M. Suzuki, T. Ida, Y. Aoyagi, Physica E **13**, 782 (2002)
36. I.W. Lyo, P. Avouris, Science **245**, 1369 (1989)